Research Article

Stanford Shateyi* and Gerald T. Marewo

Numerical solution of mixed convection flow of an MHD Jeffery fluid over an exponentially stretching sheet in the presence of thermal radiation and chemical reaction

https://doi.org/10.1515/phys-2018-0036
Received Aug 21, 2017; accepted Nov 27, 2017

Abstract: We numerically investigate a mixed convection model for a magnetohydrodynamic (MHD) Jeffery fluid flowing over an exponentially stretching sheet. The influence of thermal radiation and chemical reaction is also considered in this study. The governing non-linear coupled partial differential equations are reduced to a set of coupled non-linear ordinary differential equations by using similarity functions. This new set of ordinary differential equations are solved numerically using the Spectral Quasi-Linearization Method. A parametric study of physical parameters involved in this study is carried out and displayed in tabular and graphical forms. It is observed that the velocity is enhanced with increasing values of the Deborah number, buoyancy and thermal radiation parameters. Furthermore, the temperature and species concentration are decreasing functions of the Deborah number. The skin friction coefficient increases with increasing values of the magnetic parameter and relaxation time. Heat and mass transfer rates increase with increasing values of the Deborah number and buoyancy parameters.

Keywords: Numerical analysis, Jeffery fluid, exponentially stretching sheet, thermal radiation.

PACS: 02.60.Cb; 02.60. Lj; 47.20. Ky

1 Introduction

The numerous technological applications of non-Newtonian fluids have stimulated research within this field. Non-Newtonian fluids are technologically applied in manufacturing of plastic sheets, pharmaceutical, physiology, fiber technology, crystal growth, etc. Many models of non-Newtonian fluids have been proposed since the characteristics of non-Newtonian fluids cannot be described by a single constitutive relationship. Forced convection alone is not enough to dissipate all heat in very high-power output devices. In such cases, mixed convection will often give desired results. Mixed convection phenomena mainly occur in industrial and technological applications, such as cooling of nuclear reactors during emergency shutdowns, heat exchangers in low velocity environments, solar collectors, and electronic devices cooled by fans.

Srinivasacharya *et al.* [1] and Ishak *et al.* [2] studied mixed convention boundary layers in stagnation point flow. Ahmad *et al.* [3] analysed film flow of a micropolar fluid. Recently, Khan *et al.* [4] investigated mixed convection of a Sisko fluid in the presence of convective boundary conditions.

A Jeffrey fluid is one of the models for non-Newtonian fluids that describes the influence of the ratio of the relaxation to retardation times. Kothandapani and Srinivas [5] applied the model for MHD peristaltic flow in an asymmetric channel. Hayat *et al.* [6] examined thermal radiation effects on a Jeffrey fluid. Nadeem *et al.* [7] presented an analysis of the boundary layer flow of a Jeffrey fluid. Hayat *et al.* [8] discussed the three dimensional flow of a Jeffrey fluid when the thermal conductivity varies with temperature. Turkyilmazoglu and Pop [9] investigated the flow and heat transfer of a Jeffrey fluid near the stagnation point on a stretching/shrinking sheet.

Kavita *et al.* [10] analytically studied the effect of heat transfer of an MHD oscillatory flow of Jeffrey fluid. Khan *et al.* [11] investigated the problem of MHD boundary layer

***Corresponding Author: Stanford Shateyi:** University of Venda, Department of Mathematics, P Bag X5050, Thohoyandou 0950, South Africa; Email: stanford.shateyi@univen.ac.za
Gerald T. Marewo: University of Limpopo, Department of Mathematics & Applied Mathematics, P Bag X1106, Sovenga 0727, South Africa; Email: gtmarewo@gmail.com

flow. Bilal *et al.* [12] discussed flow of a Jeffrey nanofluid over a radially stretching sheet. Abbasi *et al.* [13] applied the homotopy analysis method to solve a Jef- frey nanofluid flow with thermal radiation and double stratification. More recently, Ali *et al.* [14] analytically and exactly studied an oscillating and incompressible MHD secondgrade fluid in porous medium. Xiao-Jun *et al.* [15] proposed a new numerical approach, embedding the differential transform and Laplace transform to solve the diffusion equation frac- tional heat transfer derivative. Xiao-Jun [16] proposed a new integral transform operator.

Ellahi *et al.* [17] discussed effects of nanoparticles to analyze Jeffrey fluid along a catheter. Hamad *et al.* [18] investigated the dynamics of a Jeffrey fluid near the stagnation point on a stretching sheet taking into account the thermal jump condition at the surface.

Recently, Das *et al.* [19] presented a numerical analysis of an electrically conducting Jeffrey fluid over a stretching sheet with partial surface slip.

Heat transfer process with radiation effects is very significant in electrical power generation, space vehicles, missiles, nuclear plants, astrophysical flows and many other applications. Little work has been done on mixed convection flow of MHD Jeffrey fluid over an exponentially stretching sheet in the presence of thermal radiation and chemical reaction. The governing equations of a Jeffrey fluid will be simplified by using a suitable similarity variable and then solved numerically by the Spectral Quasi-Linearization method (SQLM). Graphs and tables are presented to illustrate and discuss important hydrodynamic, thermal and solutal characteristics of the the flow.

2 Mathematical formulation

We consider a steady two-dimensional incompressible Jeffrey fluid over an exponentially stretching sheet. Thermal radiation and a uniform chemical reaction are significant in this study. The x-coordinate is along the stretching sheet and the y-coordinate is taken to be perpendicular to the stretching sheet. The sheet is stretched vertically with velocity $u_w = u_0 \exp\left(\frac{x}{L}\right)$, where u_0 is a constant and L is the reference length. We also assume that the sheet has surface temperature $T_w = T_\infty + T_0 \exp\left(\frac{x}{L}\right)$ and surface concentration $C_w = C_\infty + C_0 \exp\left(\frac{x}{L}\right)$, where T_0 and C_0 are constants. T_∞ and C_∞ are, respectively, the free stream temperature and concentration. The governing boundary layer equations for the model under consideration are:

$$\frac{\partial u}{\partial x} + \frac{\partial v}{\partial y} = 0, \tag{1}$$

$$u\frac{\partial u}{\partial x} + v\frac{\partial u}{\partial x} = \frac{\nu}{1+\lambda_1}\left[\frac{\partial^2 u}{\partial y^2}\right] + g\beta_T(T - T_\infty) + g\beta_c(C - C_\infty) - \frac{\delta B^2 u}{\rho} + \frac{\nu\lambda_2}{1+\lambda_1}\left(u\frac{\partial^3 u}{\partial x \partial y^2} + \frac{\partial u}{\partial y}\frac{\partial^2 u}{\partial x \partial y} - \frac{\partial u}{\partial x}\frac{\partial^2 u}{\partial y^2} + v\frac{\partial^3 u}{\partial y^3}\right), \tag{2}$$

$$u\frac{\partial T}{\partial x} + v\frac{\partial T}{\partial y} = \alpha\frac{\partial^2 T}{\partial y^2} - \frac{\partial q_r}{\partial y}, \tag{3}$$

$$u\frac{\partial C}{\partial x} + v\frac{\partial C}{\partial y} = D\frac{\partial^2 C}{\partial y^2} - k_r(C - C_\infty), \tag{4}$$

where u and v are the velocity components in the x and y directions, respectively. λ_1 is the ratio of relaxation time to retardation time, λ_2 is the retardation time, T is fluid temperature, C is fluid concentration, D is mass diffusivity, k_r is the chemical reaction rate constant, ν is kinematic viscosity, q_r is the radiative heat flux, ρ is fluid density. Also, g, β_T, β_c, α are gravitational acceleration, thermal expansion coefficient, solutal expansion coefficient, and thermal diffusivity, respectively. B is the magnetic field which is assumed to be $B = B_0 \exp(\frac{x}{L})$ where, B_0 is a constant magnetic field.

The corresponding boundary conditions for the flow model are:

$$u = u_w(x), \quad v = 0, \quad T = T_w(x), \quad C = C_w(x), \quad \text{at} \quad y = 0, \tag{5}$$

$$u \to 0, \quad \frac{\partial u}{\partial y} \to 0, T \to T_\infty, \quad C \to C_\infty, \quad \text{as} y \to \infty. \tag{6}$$

2.1 Similarity transformations

The stream function ψ is introduced such that, $u = \frac{\partial \psi}{\partial y}$, $v = -\frac{\partial \psi}{\partial x}$, and we define the non-dimensional variables

$$u = u_0 \exp\left(\frac{x}{L}\right) f'(\eta), \tag{7}$$

$$v = -\sqrt{\frac{u_0 \nu}{2L}} \exp\left(\frac{x}{2L}\right)\left[f(\eta) + \eta f'(\eta)\right],$$

$$\theta(\eta) = \frac{T - T_\infty}{T_w - T_\infty},$$

$$\phi(\eta) = \frac{C - C_\infty}{C_w - C_\infty}, \eta = y\sqrt{\frac{u_0}{2\nu L}} \exp\left(\frac{x}{2L}\right).$$

Upon substituting the similarity variables into Equations (2) - (4), we obtain:

$$f''' + \beta\left(ff'' + \frac{3}{2}(f'')^2 - \frac{1}{2}ff^{(iv)}\right) \tag{8}$$

$$+(1+\lambda_1)[ff''-2(f')^2]$$
$$+(1+\lambda_1)[2\lambda_3\theta+2\lambda_4\phi-M^2f']=0,$$

$$\left(\frac{4+3R}{6PrR}\right)\theta''+\frac{1}{2}f\theta'-f'\theta=0, \tag{9}$$

$$\frac{1}{2Sc}\phi''+\frac{1}{2}f\phi'-f'\phi-\gamma\phi=0. \tag{10}$$

The corresponding boundary conditions are

$$f(0)=0,\quad f'(0)=1,\quad \theta(0)=1,\quad \phi(0)=1, \tag{11}$$

$$f'(\infty)\to 0,\quad f''(\infty)\to 0,\quad \theta(\infty)\to 0,\quad \phi(\infty)\to 0. \tag{12}$$

Here, prime denotes differentiation with respect to η, $\beta = u_0\lambda_2/L\exp(x/L)$ is the Deborah number, $\lambda_3 = g\beta_T\exp(-2x/L)\nu L(T_w-T_\infty)$ is the thermal buoyancy parameter, $\lambda_4 = g\beta_T\exp(-2x/L)\nu L(C_w-C_\infty)$ is the solutal buoyancy parameter, $M^2 = \sigma B_0^2u_0/\rho\exp(2x/L)$, $R = 4\sigma^\star T_\infty^3/kk^\star$ is the thermal radiation parameter, $Pr = \nu/\alpha$ is the Prandtl number, $Sc = \nu/D$ is the Schmidt number, and $\gamma = k_r\exp(-x/L)$ is the chemical reaction parameter.

3 Methods of solution

3.1 An overview of the Spectral Quasi-Linearization Method (SQLM)

We illustrate the main idea of SQLM using a single n-th order nonlinear differential equation

$$F(u,u',u'',\ldots,u^{(n)})=G(x), \tag{13}$$

where $a\le x\le b$ and $',''\ldots,^{(n)}$ denote differentiation with respect to x one time, two times, …, n times. SQLM comprises two basic steps where Quasi-linearization precedes Chebyshev differentiation.

3.1.1 Quasi-linearization

Let $\mathbf{u},\mathbf{u}_r$ and $\mathbf{v}$ denote $(u,u',u'',\ldots,u^{(n)})$, $(u_r,u_r',u_r'',\ldots,u_r^{(n)})$ and $(v,v',v'',\ldots,v^{(n)})$ respectively, where $r=0,1,2,\ldots$. Taylor series expansion of (13) about $\mathbf{v}$ gives

$$\mathbf{u}\cdot\nabla F(\mathbf{v})=\mathbf{v}\cdot\nabla F(\mathbf{v})-F(\mathbf{v})+G(x), \tag{14}$$

upon neglecting higher order terms and re-arranging. Writing (14) in more details gives

$$F_{u^{(n)}}(\mathbf{v})u^{(n)}+\cdots+F_{u'}(\mathbf{v})u'+F_u(\mathbf{v})u = \mathbf{v}\cdot\nabla F(\mathbf{v})-F(\mathbf{v})+G(x), \tag{15}$$

which is an n-th order differential equation in u provided v is known. We replace $\mathbf{v}$ and $\mathbf{u}$ with $\mathbf{u}_r$ and $\mathbf{u}_{r+1}$ respectively we get

$$c_{r,n}(x)\frac{d^nu_{r+1}}{dx^n}+\cdots+c_{1,n}(x)\frac{du_{r+1}}{dx} + c_{0,n}(x)u_{r+1}=R_r(x) \tag{16}$$

where $c_{r,p}=\frac{\partial F}{u^{(p)}}(\mathbf{u}_r)$ for each $p=1,2,\ldots,n$ and

$$R_r(x)=c_{r,n}(x)\frac{d^nu_{r+1}}{dx^n}+\cdots+c_{1,n}(x)\frac{du_{r+1}}{dx} + c_{0,n}(x)u_{r+1}-F(\mathbf{u}_r)+G(x). \tag{17}$$

Hence quasi-linearization replaces the non-linear differential equation (13) with its linear counterpart (16).

3.1.2 Chebyshev differentiation

Before we apply Chebyshev differentiation on (16), we do the following:

1. If the physical domain is infinite or semi-infinite, we truncate it to a finite one $[a,b]$ but such that $|b-a|$ is large enough for the boundary conditions at the end points to still apply.
2. Use the change of variable $x(\xi)=[a+b+(b-a)\xi]/2$ to transform the differential equation (16) on the physical domain $[a,b]$ to its counterpart

$$c_{r,n}(\xi)\alpha^n\frac{d^nu_{r+1}}{d\xi}+\cdots+c_{1,n}(\xi)\alpha^1\frac{du_{r+1}}{d\xi} + c_{0,n}(\xi)\alpha^0u_{r+1}=R_r(x(\xi)), \tag{18}$$

   on the computational domain $[-1,1]$, where $\alpha = 2/(b-a)$.
3. On $[-1,1]$ define grid points $\xi_0,\xi_1,\ldots,\xi_N$ by $\xi_j=\cos(\pi j/N)$ for each $j=0,1,\ldots,N$.

Chebyshev differentiation evaluates the p-th derivative of u with respect to ξ at $\xi=\xi_j$ using the formula

$$\frac{d^pu}{d\xi}(\xi_j)=\sum_{k=0}^{N}[\hat{D}^p]_{jk}u(\xi_k), \tag{19}$$

where $\hat{D}$ is the $(N+1)\times(N+1)$ Chebyshev differentiation matrix [20]. If we evaluate Equation (18) at $\xi=\xi_j$ for each

$j = 0, 1, \ldots, N$ and then evaluate each derivative using Formula (19), we end up with a linear system

$$A\begin{pmatrix} u(\xi_0) \\ u(\xi_1) \\ \vdots \\ u(\xi_N) \end{pmatrix} = \begin{pmatrix} R_r(x(\xi_0)) \\ R_r(x(\xi_1)) \\ \vdots \\ R_r(x(\xi_N)) \end{pmatrix} \tag{20}$$

where A is a function of D. Upon solving (20) we get u at each grid point and

$$u(\xi) = \sum_{j=0}^{N} u(\xi_j) L_j(\xi), \tag{21}$$

for any $\xi \in [-1, 1]$, where L_j is the Lagrange polynomial of degree N associated with node ξ_j. Since (21) is the solution of (18), if we write ξ in terms of x then we get a solution $u(x)$ of the original differential equation (13).

3.2 Application of SQLM to current problem

If Equation (8) is written in the compact form of (13), we get

$$F(\mathbf{u}) = 0, \tag{22}$$

where $\mathbf{u} = (f, f', f'', f''', \theta, \phi)$. Upon applying Quasi-linearization on (22) we get

$$\begin{aligned} &a_{0,r} f_{r+1} + a_{1,r} f'_{r+1} + a_{2,r} f''_{r+1} + a_{3,r} f'''_{r+1} \\ &+ a_{4,r} f^{(iv)}_{r+1} + a_{5,r} \theta_{r+1} + a_{6,r} \phi_{r+1} = R^{(1)}_r, \end{aligned} \tag{23}$$

where

$$\begin{aligned} a_{0,r} &:= F_f(\mathbf{u}_r) = \beta(f''_r - \frac{1}{2} f^{(iv)}_r) + (1 + \lambda_1) f''_r, \\ a_{1,r} &:= F_{f'}(\mathbf{u}_r) = (1 + \lambda_1)(-M^2 - 4 f'_r)) \\ a_{2,r} &:= F_{f''}(\mathbf{u}_r) = \beta(f_r + 3 f''_r) + (1 + \lambda_1) f_r, \\ a_{3,r} &:= F_{f'''}(\mathbf{u}_r) = 1, \\ a_{4,r} &:= F_{f^{(iv)}}(\mathbf{u}_r) = -\frac{\beta}{2} f_r \\ a_{5,r} &:= F_{\theta}(\mathbf{u}_r) = 2(1 + \lambda_1)\lambda_3, \\ a_{6,r} &:= F_{\phi}(\mathbf{u}_r) = 2(1 + \lambda_1)\lambda_4 \\ R^{(1)}_r &= f_r f''_r + \frac{3}{2}\beta(f''_r)^2 - 2(f'_r)^2\lambda_1 - 2(f'_r)^2 \\ &\quad - \frac{1}{2}\beta f_r f^{(iv)}_r + \beta f_r f''_r + \lambda_1 f_r f''_r \end{aligned}$$

Similarly, Quasi-linearization transforms (9) to

$$\begin{aligned} &b_{0,r} f_{r+1} + b_{1,r} f'_{r+1} + b_{2,r} \theta_{r+1} \\ &+ b_{3,r} \theta'_{r+1} + b_{4,r} \theta'' = R^{(2)}_r, \end{aligned} \tag{24}$$

where

$$\begin{aligned} b_{0,r} &:= \frac{1}{2}\theta'_r,\ b_{1,r} := -\theta_r,\ b_{2,r} := -f'_r,\ b_{3,r} := \frac{1}{2} f_r, \\ b_{4,r} &:= \frac{4 + 3R}{6Pr\,R},\ R^{(2)} = \frac{1}{2} f_r \theta'_r - f'_r \theta_r. \end{aligned}$$

Proceeding in a similar manner also transforms (10) to

$$\begin{aligned} &c_{0,r} f_{r+1} + c_{1,r} f'_{r+1} + c_{2,r} \phi_{r+1} \\ &+ c_{3,r} \phi'_{r+1}, + c_{4,r} \phi'' = R^{(3)}_r \end{aligned} \tag{25}$$

where

$$\begin{aligned} c_{0,r} &:= \frac{1}{2}\phi'_r,\ c_{1,r} := -\phi_r,\ c_{2,r} := -f'_r - \gamma, \\ c_{3,r} &:= \frac{1}{2} f_r,\ c_{4,r} := \frac{1}{2Sc},\ R^{(2)} = \frac{1}{2} f_r \phi'_r - f'_r \phi_r \end{aligned}$$

Equations (23), (24) and (25) are subject to boundary conditions

$$f_{r+1}(0) = 0,\ f'_{r+1}(0) = 1,\ f'_{r+1}(\infty) = 0,\ f''_{r+1}(\infty) = 1, \tag{26}$$

$$\theta_{r+1}(0) = 1,\ \theta_{r+1}(\infty) = 0, \tag{27}$$

$$\phi_{r+1}(0) = 1,\ \phi_{r+1}(\infty) = 0, \tag{28}$$

respectively. Chebyshev differentiation replaces the differential equations (23), (24) and (25) with a single linear system

$$A\mathbf{U}_{r+1} = \mathbf{R}_r, \tag{29}$$

where

$$A = \begin{pmatrix} A^{(11)} & A^{(12)} & A^{(13)} \\ A^{(21)} & A^{(22)} & O \\ A^{(31)} & O & A^{(33)} \end{pmatrix}, \quad \mathbf{U}_{r+1} = \begin{pmatrix} \mathbf{F}_{r+1} \\ \Theta_{r+1} \\ \Phi_{r+1} \end{pmatrix}, \tag{30}$$

$$\mathbf{R}_r = \begin{pmatrix} \mathbf{R}^{(1)}_r \\ \mathbf{R}^{(2)}_r \\ \mathbf{R}^{(3)}_r \end{pmatrix}$$

$$\begin{aligned} A^{(11)} &= \text{diag}\left\{-\frac{\beta}{2}\mathbf{F}_r\right\}\hat{D}^4 + \hat{D}^3 + \text{diag}\{\beta(\mathbf{F}_r + 3\mathbf{F}''_r) \\ &+ (1 + \lambda_1)\mathbf{F}_r\}\hat{D}^2 + [-(1 + \lambda_1)M^2 I - 4(1 + \lambda_1)\mathbf{F}'_r]\hat{D} + \\ &\text{diag}\left\{\beta(\mathbf{F}''_r - \frac{1}{2}\mathbf{F}^{(iv)}_r) + (1 + \lambda 1)\mathbf{F}''_r\right\}, \end{aligned}$$

$$\begin{aligned} A^{(12)} &= 2(1 + \lambda_1)\lambda_3 I,\ A^{(13)} = 2(1 + \lambda_1)\lambda_4 I \\ \mathbf{R}^{(1)}_r &= \mathbf{F}_r \circ \mathbf{F}''_r + \frac{3}{2}\beta\mathbf{F}''_r \circ \mathbf{F}''_r - 2\lambda_1 \mathbf{F}'_r \circ \mathbf{F}'_r \\ &\quad - 2\mathbf{F}'_r \circ \mathbf{F}'_r - \frac{\beta}{2}\mathbf{F}_r \circ \mathbf{F}^{(iv)}_r \end{aligned}$$

$$+\beta\mathbf{F}_r\circ\mathbf{F}_r''+\lambda_1\mathbf{F}_r\circ\mathbf{F}_r'',$$

$$A^{(21)}=\operatorname{diag}\{-\Theta_r\}\hat{D}+\operatorname{diag}\left\{\frac{1}{2}\Theta_r'\right\},$$

$$A^{(22)}=\frac{4+3R}{6\,Pr\,R}\hat{D}^2+\operatorname{diag}\left\{\frac{1}{2}\mathbf{F}_r\right\}\hat{D}+\operatorname{diag}-\mathbf{F}_r',$$

$$\mathbf{R}_r^{(2)}=\frac{1}{2}\mathbf{F}_r\circ\Theta_r'-\mathbf{F}_r'\circ\Theta_r,$$

$$A^{(31)}=\operatorname{diag}\{-\Phi_r\}\hat{D}+\operatorname{diag}\left\{\frac{1}{2}\Phi_r'\right\},$$

$$A^{(33)}=\frac{1}{Sc}\hat{D}^2+\operatorname{diag}\left\{\frac{1}{2}\mathbf{F}_r\right\}\hat{D}+\operatorname{diag}\{-\mathbf{F}_r'\}-\gamma I,$$

$$\mathbf{R}_r^{(2)}=\frac{1}{2}\mathbf{F}_r\circ\Phi_r'-\mathbf{F}_r'\circ\Phi_r,$$

$$\mathbf{F}_r=[f_r(\xi_0)\,f_r(\xi_1)\,\ldots\,f_r(\xi_N)]^T,$$

$$\Theta_r=[\theta_r(\xi_0)\,\theta_r(\xi_1)\,\ldots\,\theta_r(\xi_N)]^T.$$

$\Phi_r=[\phi_r(\xi_0)\,\phi_r(\xi_1)\,\ldots\,\phi_r(\xi_N)]^T$, I is the $(N+1)\times(N+1)$ identity matrix and

$$\operatorname{diag}\{u_0,u_1,\ldots,u_N\}=\begin{pmatrix}u_0 & & & \\ & u_1 & & \\ & & \ddots & \\ & & & u_N\end{pmatrix}$$

is an $(N+1)\times(N+1)$ diagonal matrix. The linear system (29) is subject to boundary conditions

$$f_{r+1}(\xi_N)=0,\ \sum_{k=0}^{N}\hat{D}_{Nk}f(\xi_k)=1, \tag{31}$$

$$\sum_{k=0}^{N}\hat{D}_{0k}f(\xi_k)=0,$$

$$\sum_{k=0}^{N}[\hat{D}^2]_{0k}f(\xi_k)=0, \tag{32}$$

$$\theta_{r+1}(\xi_N)=1,\ \theta_{r+1}(\xi_0)=0, \tag{33}$$

$$\phi_{r+1}(\xi_N)=1,\ \phi_{r+1}(\xi_0)=0. \tag{34}$$

Solution of the linear system (29) is preceded by the following:

1. We include boundary conditions (32) through (34) in a manner similar to that as in paper by Motsa *et al.* [21].
2. We choose initial approximations as

   $$f_0(\eta)=1-e^{-\eta},\ \theta_0(\eta)=e^{-\eta},\ \phi_0(\eta)=e^{-\eta},$$

   so that we satisfy boundary conditions (26) through (28).

Since $\mathbf{U}_0$ is now known, if we solve Equation (29) for each $r=0,1,\cdots$ we get subsequent approximations $\mathbf{U}_1,\mathbf{U}_2,\cdots$.

4 Results and discussion

A parametric study is conducted and the results are presented in both graphical and tabular forms, as well as being discussed. The numerical results are iteratively generated by the Spectral Quasi-Linearization Method (SQLM) for the parameters that are significant in the current work. It is remarked that the SQLM results presented in this work were obtained using $N=50$ allocation points with the infinity value n_∞ taken as 30. The tolerance level was set to be $\epsilon=10^{-8}$. The following are the default values for pertinent parameters considered in this study:
$\beta=0.5,\lambda_1=0.3,\lambda_3=0.5,\lambda_4=0.5,M=1,R=1,Pr=0.71,Sc=0.22$. The number of collocation points N was fixed as the smallest values of N which gives a consistent solution with the stipulated tolerance level ε. Figure 1 shows the convergence and stability of the solutions generated by the SQLM. We can observe from this figure that convergence is realised at as low as 5 iterations which shows that this method as equally good as other numerical and analytical methods such as the variational iteration method or the homotopy perturbation method.

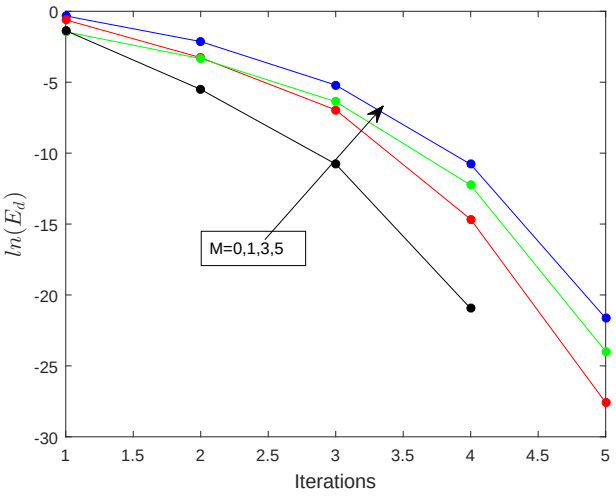

Figure 1: Logarithm of the SQLM error when varying M.

Table 1 presents a comparison between SQLM approximate results and *bvp4c* results for default values of magnetic parameter M. We observe that there is an excellent agreement between the results from the two methods.

The influences of the Deborah number, the ratio of the relaxation to retardation times, thermal buoyancy, magnetic and thermal radiation parameters on the skin friction coefficient, and Nusselt and Sherwood numbers are displayed in Tables 2, 3 and 4, respectively. We observe in

Table 1: SQLM results of $-f''(0)$, $-\theta'(0)$ to $bvp4c$ results for different values of the magnetic parameter

	$-f''(0)$		$-\theta'(0)$	
M	$bvp4c$	SQLM	$bvp4c$	SQLM
1	1.08728035	1.08728035	1.90242286	1.90242286
3	2.58326872	2.58326872	1.51912627	1.51912627
5	4.28753502	4.28753502	1.15798805	1.15798805

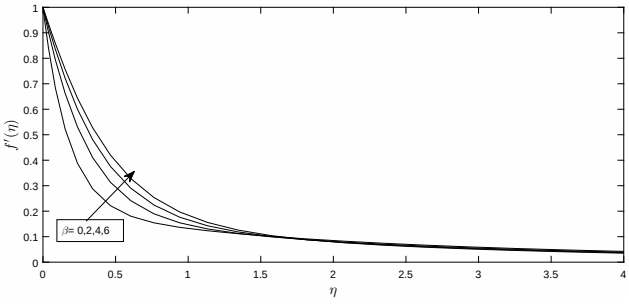

Figure 2: Effects of the Deborah number on dimensionless velocity.

these respective tables that the Deborah number has very significant influence on skin friction coefficient and Nusselt and Sherwood numbers. We observe that the skin friction coefficient is reduced when the Deborah number β increases. Increasing the value of β implies that fluid elasticity is enhanced at the same time reducing viscosity, thus reducing the frictional force on the surface. However, the Nusselt number and Sherwood number are enhanced by increasing values of the Deborah number. Increasing the values of the ratio of relaxation time to retardation time significantly increases the skin friction coefficient but at the same time reduces the Nusselt and Sherwood numbers. The fluid particles need much more time to come back from a perturbed system to an equilibrium system, thus increasing frictional force on the surface at the same time reducing the rates of heat and mass transfer on the wall surface. Increasing the buoyancy forces, as expected, has significant effects on the skin friction coefficient, Nusselt number and Sherwood numbers. The skin friction coefficient is reduced with enhanced values of buoyancy forces, whereas the opposite effect is encountered on the rates of heat and mass transfer on the surface. We also observe in these tables that the skin friction coefficient increases with increasing values of the magnetic parameter, but the rates of heat and mass transfer are reduced. Lastly, we see in Table 2 that increasing the value of thermal radiation enhances the skin friction coefficient as well as the Nusselt number but has little effect on the Sherwood number.

Figure 2 depicts the influence of the Deborah number, β, on velocity profiles. As β depends on the retarda-

Table 2: Values of skin friction coefficient, for different values of $\beta; \lambda_1; \lambda_3; M; R$.

β	λ_1	λ_3	M	R	$-f''(0)$
0	0.1	0.5	1	1	4.67874200
2					2.66663467
4					2.04581283
	0				2.23971109
	3				4.39534222
	6				5.79030365
		0			2.75976983
		1			2.32371133
		3			1.4420629
			0		0.42483935
			2		1.62729681
			4		3.46315415
				1	0.80765164
				3	0.83641333
				5	0.84491745

Table 3: Values of Nusselt number for different values of $\beta; \lambda_1; \lambda_3; M; R$.

β	λ_1	λ_3	M	R	$-\theta'(0)$
0	0.1	0.5	1	1	0.38872137
2					0.43632230
4					0.46514657
	0				0.46793594
	3				0.39080196
	6				0.36932417
		0			0.34822841
		1			0.50505217
		3			0.63587307
			0		0.74230941
			2		0.56420731
			4		0.36408773
				1	0.68553175
				3	0.90558795
				5	0.97707718

Table 4: Values of Sherwood number for different values of $\beta; \lambda_1; \lambda_3; M; R$.

β	λ_1	λ_3	M	R	$-\phi(0)$
0	0.1	0.5	1	1	0.78619180
2					0.81212278
4					0.82661696
	0				0.82689792
	3				0.78754319
	6				0.77516374
		0			0.80023181
		1			0.83418647
		3			0.88378152
			0		0.93356195
			2		0.85992176
			4		0.78907194
				1	0.90836827
				3	0.90288648
				5	0.90135709

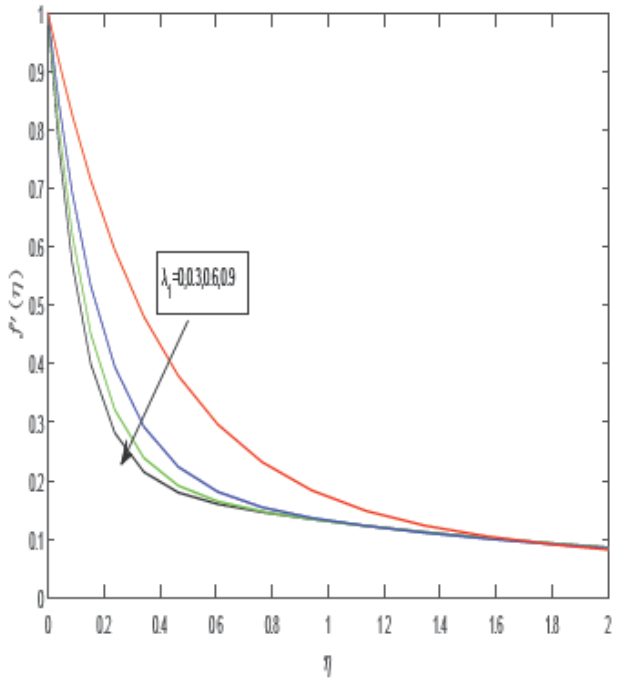

Figure 3: Variation of the relaxation time parameter on dimensionless velocity.

tion time λ_2, increasing the value of β corresponds to increase in the retardation time. Physically, elasticity is enhanced by an increase in the retardation time. It is noted that elasticity and viscosity effects are inversely proportional to each other so the fluid velocity is enhanced by a decrease in viscosity. This explains why the velocity increases as the value of the Deborah number increases as can be clearly observed in Figure 2.

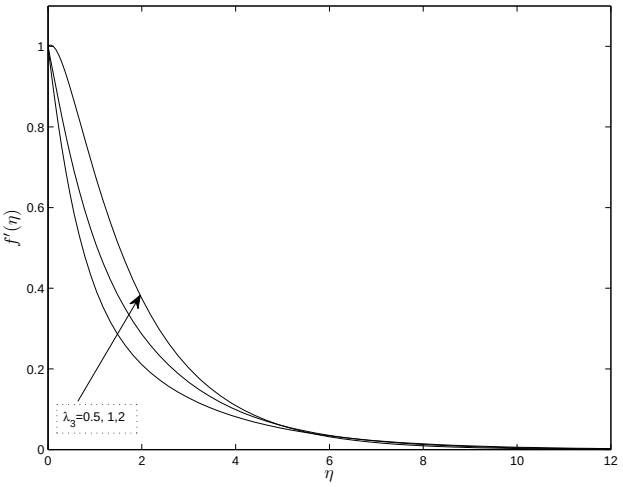

Figure 4: Variation of thermal buoyancy parameter on dimensionless velocity.

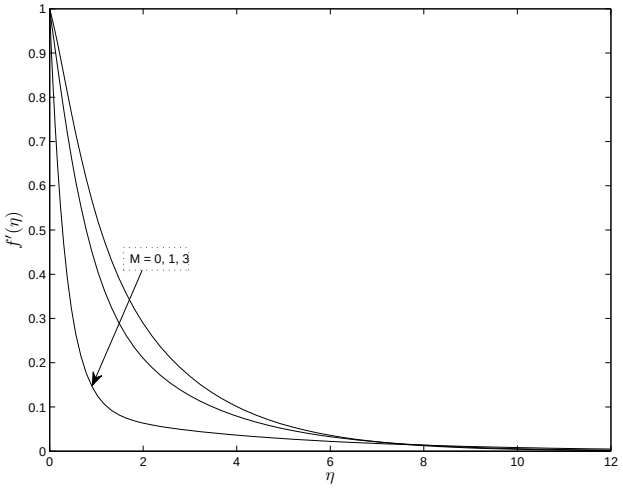

Figure 5: Effect of the magnetic parameter on the velocity distribution

The influence of the ratio of relaxation time to retardation time, λ_1, on the velocity is illustrated in Figure 3. Physically, an increase in λ_1 corresponds to increase in the relaxation time and/or a decrease in the retardation time. This then means that fluid particles need much more time to come back from a disturbed system to an equilibrium system. Thus the velocity decreases with increasing values of λ_1 as can been seen in Figure 3.

Figure 4 displays effects of the thermal buoyancy parameter λ_3 on velocity profiles. As expected, it is clearly observed that the velocity profiles are enhanced by increasing the value of λ_3. Increasing λ_3 makes the buoyancy force stronger and stronger and this in turn increases

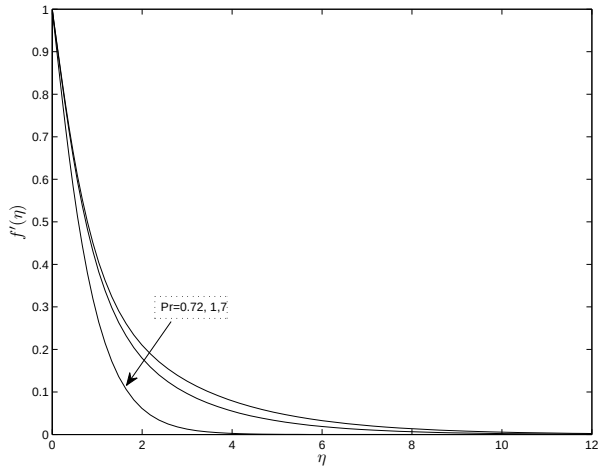

(a)

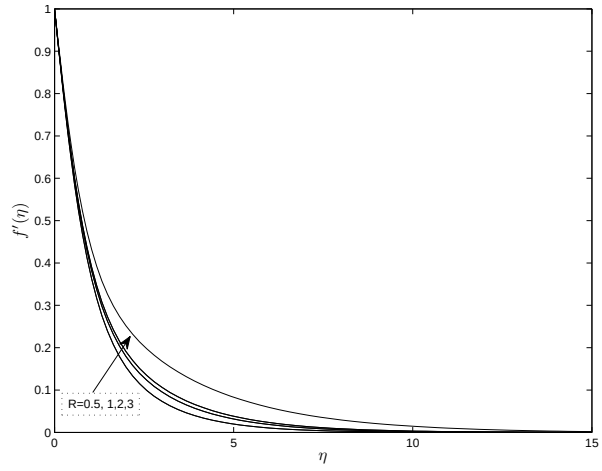

(b)

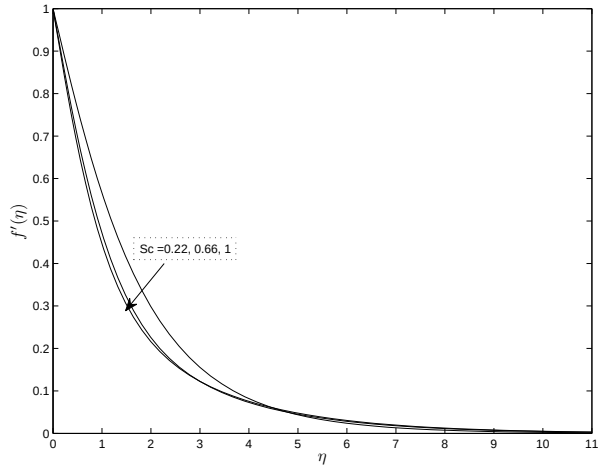

(c)

Figure 6: Variation of the Prandtl number (a), thermal radiation number (b) and the Schmidt number on the velocity profiles

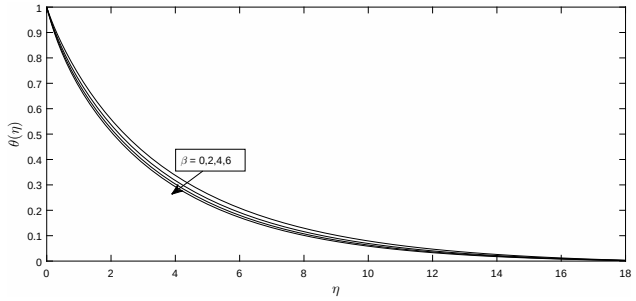

Figure 7: Effects of the Deborah number on dimensionless temperature.

the velocity profiles. The effect of the magnetic parameter on the velocity distribution is depicted in Figure 5. An increase in the strength of the magnetic field produces a drag force which reduces the fluid velocity. The application of a controlled transverse magnetic field can be used as a stabilizing mechanism to boundary layer flow. This can also be used to delay the transition from laminar to turbulent flow.

Figure 6 shows variation of the Prandtl number, thermal radiation number and Schmidt number on velocity profiles. A small value of the Prandtl number, $Pr << 1$, means that thermal diffusivity dominates while a large value, $Pr >> 1$, means that the momentum diffusivity dominates the flow behavior. This explains why the fluid velocity is greatly reduced when the values of the Prandtl number are increased as can be clearly seen in Figure 6(a). Figure 6 (b) clearly indicates that the fluid velocity profiles and boundary layer thickness increase with an increase in thermal radiation parameter (R). However, the velocity profiles and boundary layer thickness are greatly reduced by increasing values of the Schmidt number. Physically, Schmidt number is a dimensionless parameter which represents the ratio of momentum diffusion to mass diffusion in fluid. When the Schmidt number is large, it means that the momentum is transported by molecular means across a liquid much more effectively than by species. Thus the fluid becomes heavier thereby reducing the fluid velocity as can clearly be observed in Figure 6 (c).

The effect of the Deborah number on the temperature is depicted in Figure 7. It is observed that increasing the value of the Deborah number yields a reduction in both temperature and thermal boundary layer thickness. Figure 8 depicts the influences of the thermal buoyancy parameter, magnetic parameter and thermal radiation R on the temperature profiles. We observe that temperature decreases with increasing values of the thermal buoyancy force. Large values of λ_3 produce large buoyancy force which in turn produces large kinetic energy. Thus the tem-

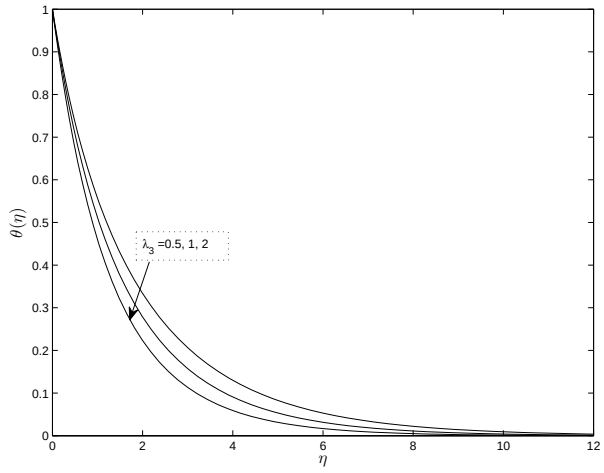

(a)

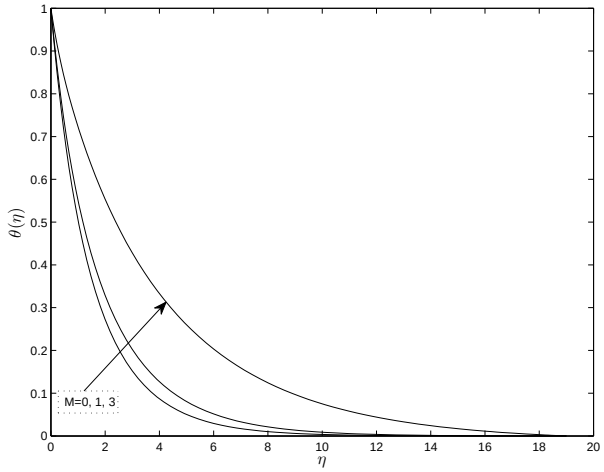

(b)

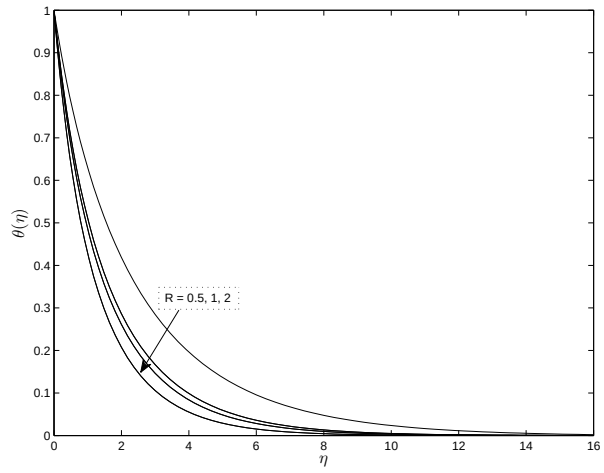

(c)

Figure 8: Variation of the thermal buoyancy parameters (a), magnetic parameter (b) and thermal radiation (c) on the temperature profiles

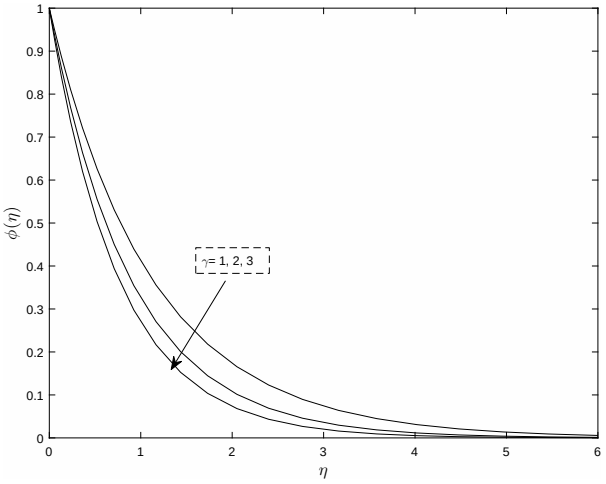

(a)

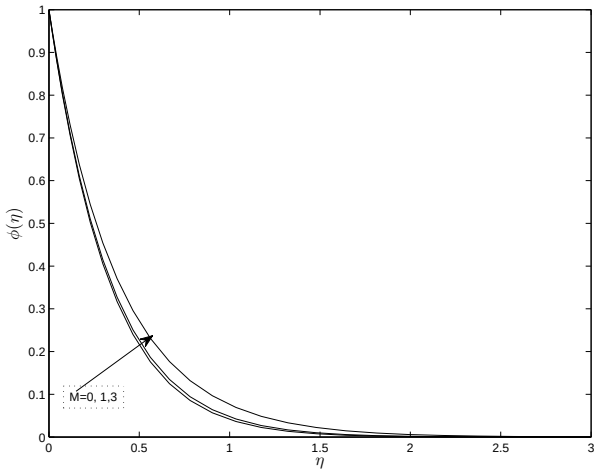

(b)

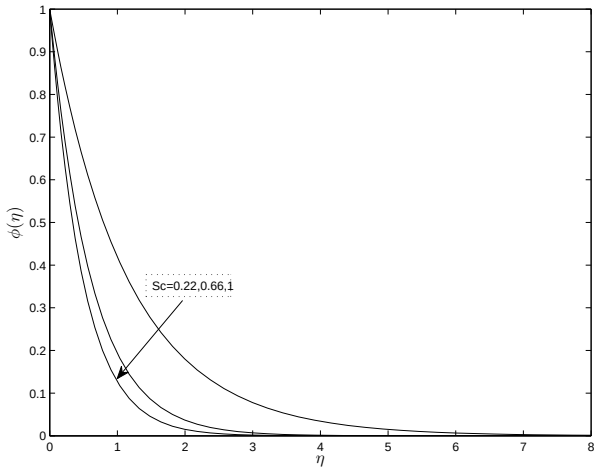

(c)

Figure 9: Variation of chemical reaction (a), magnetic parameter (b) and Schmidt number (c) on the concentration profiles

perature and thermal boundary layer are reduced as λ_3 increases. Increasing the strength of the magnetic field enhances the fluid temperature as can be seen in Figure 8(b). Increasing the value of the thermal radiation R has a tendency to increase conduction effects. Thus higher values of R imply higher surface flux, therefore reducing the temperature at each point away from the surface. This can be seen in Figure 7(c). It is observed that the thermal boundary layer thickness decreases as the value of R increases.

Figure 9 displays the influence of chemical reaction, the magnetic parameter and the Schmidt number on concentration profiles. As expected, the concentration profiles are reduced with increasing values of chemical reaction parameter. The velocity of the fluid is reduced as the magnetic field parameter increases this in turn enhances the species concentration. This explains why the concentration profile and solutal boundary layer increase as the magnetic parameter increases. Lastly, we observe that the concentration and the solutal boundary layer are significantly reduced as the value of the Schmidt number increases. This is because when the Schmidt number is large, momentum is transported by molecular means across liquid much more effectively than by species.

5 Conclusions

The current study investigated the problem of mixed convection flow of an MHD Jeffery fluid in the presence of thermal radiation and chemical reaction. The following are the main observations of this investigation:

1. Increases in the values of the Deborah number β, lead to increasing values of the velocity profiles as well as momentum boundary layer thickness. However, the fluid temperature and species concentration are decreasing functions of the Deborah number.
2. The fluid velocity is found to be an increasing function of the buoyancy parameters (λ_3, λ_4), thermal radiation and retardation time. Meanwhile, fluid velocity is found to decrease with increasing values of the magnetic parameter, Prandtl and Schmidt numbers.
3. Fluid temperature as well as the thermal boundary layer thickness increase with increasing values of the magnetic parameter and retardation time, but decreases with increasing values of the Deborah number, Prandtl number, thermal radiation and buoyancy parameter.
4. The species concentration and the solutal boundary layer thickness increase with increasing values of the magnetic parameter and retardation time. However, the opposite influences are observed when values of the Deborah number, buoyancy and chemical reaction parameters are increased.
5. We also observe that the SQLM is a very fast reliable method that can converge after as few as five iteration.

References

[1] Srinivasacharya D., Reddy S., Mixed convection heat and mass transfer over a vertical plate in a power-law fluid-saturated porous medium with radiation and chemical reaction effects, Heat Transf.-Asian Res., 2013, 42(6), 485-499.
[2] Ishak A., Nazar R., Pop I., Mixed convection boundary layers in the stagnation-point flow toward a stretching vertical sheet, Meccanica, 2008, 41, 509-518.
[3] Ahmad K., Hanoul Z., Ishak A., Mixed convection Jeffrey fluid flowover an exponentially stretching sheet with magnetohydrodynamic effect, AIP Adv., 2016, 6, 035024
[4] Khan M., Malik M., Munir A., Mixed convection heat transfer to Sisko fluid over a radially stretching sheet in the presence of convective boundary conditions, AIP Adv., 2015, 5, 087178
[5] Kothandapani M., Srinivas S., Peristaltic transport of a Jeffrey fluid under the effect of magnetic field in an asymmetric channel, Int. J. Non-Linear Mech., 2008, 43, 915-924.
[6] Hayat T., Shehzad S.A., Qasim M., Obaida S., Thermal radiation effects on mixed convection stagnation-point flow in a Jeffery fluid, Z. Naturforsch., 2011, 66a, 606-614.
[7] Nadeem S., Zaheer S., Fang T., Effects of thermal radiation on the boundary layer flow of a Jeffrey fluid over an exponentially stretching surface, Numer. Algor., 2011, 57, 187-205.
[8] Hayat T., Shehzad S.A, Alsaedi A., Three-dimensional stretched flow of Jeffrey fluid with variable thermal conductivity and thermal radiation, Appl. Math. Mech., 2013, 34(7), 823-832.
[9] Turkyilmazoglu M., Pop I., Exact analytical solutions for the flow and haet transfer near the stagnation point on a stretching/sheet in a Jeffrey fluid, Int. J. Heat Mass Transf., 2013, 57, 82-88.
[10] Kavita K., Ramakrishna Prasad K., Aruna Kumari B., Influence of heat transfer on MHD oscillatory flow of Jeffrey fluid in a channel, Advances in Applied Science Research, 2012, 3(4), 2312-2325.
[11] Khan Y., Abdou, M.A, Faraz N, Yildirim A, Wu Q., Numerical Solution of MHD Flow over a Nonlinear Porous Stretching Sheet, Iran. J. Chem. Chem. Eng, 2012, 31(3), 125-132.
[12] Bilal Ashraf M., Hayat T., Alsaedi A., Shehzad S.A., Convective heat and mass transfer in MHD mixed convection flow of Jeffrey nanofluid over a radially stretching surface with thermal radiation, J. Cent. South Univ. 2015, 22, 1114-1123.
[13] Abbasi F.M., Shehzad S.A., Hayat T., Alhuthali M.S., Mixed convection flow of jeffrey nanofluid with thermal radiation and double stratification, J. Hydrodyn., 2016, 28(5), 840-849.
[14] Ali F., Sheikh N.A., Saqib M., Khan A., Hidden Phenomena of an MHD Unsteady Flow in Porous Medium with Heat Transfer, Non-

linear Sci. Lett. A, 2017, 8(1), 101-116.
[15] Xiao-Jun Y., Tenreiro Machadoc J.A., Baleanud D., Gao F., A new numerical technique for local fractional diffusion equation in fractal heat transfer, J. Nonlinear Sci. Appl. 2016, 9, 5621-5628.
[16] Xiao-Jun Y., A new integral transform operator for solving the heat-diffusion problem, Appl. Math. Lett., 2017, 64, 193-197.
[17] Ellahi R., Rahman S.U., Nadeem S., Blood flow of Jeffrey fluid in a catherized tapered artery with the suspension of nanoparticles, Phys. Lett. A, 2014, 378, 2973-2980.
[18] Hamad M.A.A., Abd El-Gaied S.M., Khan W.A., Thermal Jump Effects on Boundary Layer Flow of a Jeffrey Fluid Near the Stagnation Point on a Stretching/Shrinking Sheet with Variable Thermal Conductivity, J. Fluids, 2013, 749271
[19] Das K., Acharya N., Kundu P. K., Radiative flow of MHD Jeffrey fluid past a stretching sheet with surface slip and melting heat transfer, Alex. Eng. J., 2015, 54, 815-821.
[20] Trefethen L.N., Spectral Methods in MATLAB, SIAM, 2000.
[21] Motsa S.S., Sibanda P., Ngnotchouye J.M., Marewo G.T., A Spectral Relaxation Approach for Unsteady Boundary-Layer Flow and Heat Transfer of a Nanofluid over a Permeable Stretching/Shrinking Sheet, Adv. Math. Phys., 2014, 564942